

1 **Title: Recombinant Spidroins Fully Replicate Primary Mechanical Properties**
2 **of Natural Spider Silk**

3 *Authors:* Christopher H. Bowen,¹ †, Bin Dai^{1,} †, Cameron Sargent¹, Wenqin Bai¹, Pranay
4 Ladiwala¹, Huibao Feng¹, Wenwen Huang³, David Kaplan³, Jonathan Galazka⁴, Fuzhong
5 Zhang^{1,2,*}

6

7 **Affiliations:**

8 ¹Department of Energy, Environmental and Chemical Engineering,

9 ²Institute of Materials Science & Engineering,

10 Washington University in St. Louis, Saint Louis, MO 63130, USA

11 ³ TBA

12 ⁴ Space Biosciences Division, Ames Research Center, National Aeronautics and Space

13 Administration, Mountain View, CA 94035, USA

14 † These authors contributed equally.

15 *Correspondence to: fzhang@seas.wustl.edu

16

17

18

19

20

21

22

23

24 **Abstract:**

25 Dragline spider silk is among the strongest and toughest bio-based materials, capable of
26 outperforming most synthetic polymers and even some metal alloys.^{1,2,3,4} These properties
27 have gained spider silk a growing list of potential applications that, coupled with the
28 impracticalities of spider farming, have driven a decades-long effort to produce
29 recombinant spider silk proteins (spidroins) in engineered heterologous hosts.² However,
30 these efforts have so far been unable to yield synthetic silk fibers with mechanical
31 properties equivalent to natural spider silk, largely due to an inability to stably produce
32 highly repetitive, high molecular weight (MW) spidroins in heterologous hosts.^{1,5} Here we
33 address these issues by combining synthetic biology techniques with split intein (SI)-
34 mediated ligation for the bioproduction of spidroins with unprecedented MW (556 kDa),
35 containing 192 repeat motifs of the *Nephila clavipes* MaSp1 dragline spidroin. Fibers spun
36 from these synthetic spidroins display ultimate tensile strength (σ), modulus (E),
37 extensibility (ϵ), and toughness (U_T) of 1.03 ± 0.11 GPa, 13.7 ± 3.0 GPa, $18 \pm 6\%$, and $114 \pm$
38 51 MJ/m³, respectively—equivalent to the performance of natural *N. clavipes* dragline silk.⁶
39 This work demonstrates for the first time that microbially produced synthetic silk fibers
40 can match the performance of natural silk fibers by all common metrics (σ , E, ϵ , U_T),
41 providing a more dependable source of high-strength fibers to replace natural spider silks
42 for mechanically demanding applications. Furthermore, our biosynthetic platform can be
43 potentially expanded for the assembly and production of other protein-based materials
44 with high MW and repetitive sequences that have so far been impossible to synthesize by
45 genetic means alone.

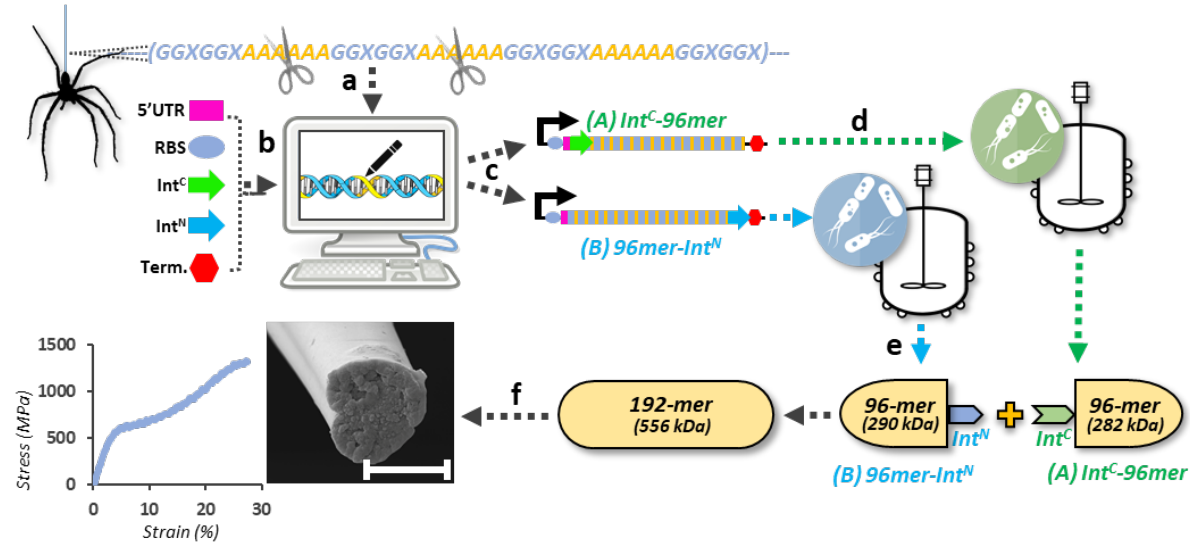
47

48 **Main Text:**

49 Dragline spidroins are typically very large (200-350 kDa), highly repetitive proteins,
50 containing hundreds of tandem repeats of glycine and alanine-rich sequences.^{1,7} As with most
51 polymers, the size of these spidroins is expected to positively correlate with tensile strength due
52 to an increased density of interchain interactions and entanglements and fewer chain-end
53 defects.^{8,5} Indeed, previous work has demonstrated a clear correlation between MW and strength
54 for recombinant *N. clavipes* dragline fibers, with the largest spidroin (96-mer, 285 kDa) yielding
55 the strongest recombinant fiber reported to date (~550 MPa).⁵ However, despite the apparent
56 need for even larger spidroins to yield natural strength fibers (1.1 GPa for *N. clavipes* dragline)⁶,
57 dragline spidroins larger than 285 kDa have yet to be produced in quantities sufficient for fiber
58 testing due to major challenges in recombinant production of high MW spidroins (e.g. instability
59 of long, highly repetitive DNA/mRNA sequences in heterologous hosts, translation inhibition by
60 complex mRNA secondary structures, high demands for glycine and alanine tRNAs, overall
61 metabolic burden).⁵

62

63



64

65 **Figure 1. Process schematic for split intein-mediated ligation of spider silk proteins with**
 66 **unprecedented molecular weight and mechanical properties. (a)** The highly repetitive core of
 67 natural *N. clavipes* dragline silk protein MaSp1 (shown as an idealized peptide sequence) is
 68 reduced to a single repeat unit (1-mer). **(b)** The 1-mer DNA sequence is combined *in silico* with
 69 5' UTR, RBS, and split intein (SI) sequences, which are then computationally optimized for
 70 microbial production. **(c)** The optimized DNA sequences are assembled through our
 71 standardized SI-Brick system to yield complementary Int^C- or Int^N-flanked 96-mer constructs
 72 which are **(d)** transformed to *E. coli* for bioproduction. **(e)** Cell cultures are mixed and lysed to
 73 initiate SI-mediated covalent ligation of 96-mer spidroins to yield a 192-mer, 556 kDa product.
 74 **(f)** Ligated product is purified and spun into fibers for mechanical testing. Scale bar indicates 5
 75 μm.

76

77 To confront these challenges, we envisioned using split intein (SI)-mediated reactions to
 78 post-translationally ligate the largest spidroins that can be stably expressed in engineered
 79 *Escherichia coli* (i.e. 96-mer, Fig. 1). SIs are peptide auto processing domains that, when fused

80 to separately expressed proteins, catalyze spontaneous splicing reactions, covalently linking their
81 fusion partners via a peptide bond and leaving only a few residues (6 amino acids in this case) at
82 the ligation site.⁹ In this context, these residues are unlikely to affect the properties of the much
83 larger ligated spidroins (6720 amino acids). Given the tendency of large silk sequences to form
84 inclusion bodies in microbial hosts, we employed a recently engineered SI pair (Cfa) that retains
85 catalytic activity in the presence of 8 M urea, a denaturant often used to extract and solubilize
86 spidroins from heterologous hosts.¹⁰ Thus, ligating an N-intein fused 96-mer (^N96) with a C-
87 intein fused 96-mer (96^C) spidroin would yield a 556 kDa, 192-mer spidroin (Fig 1e).

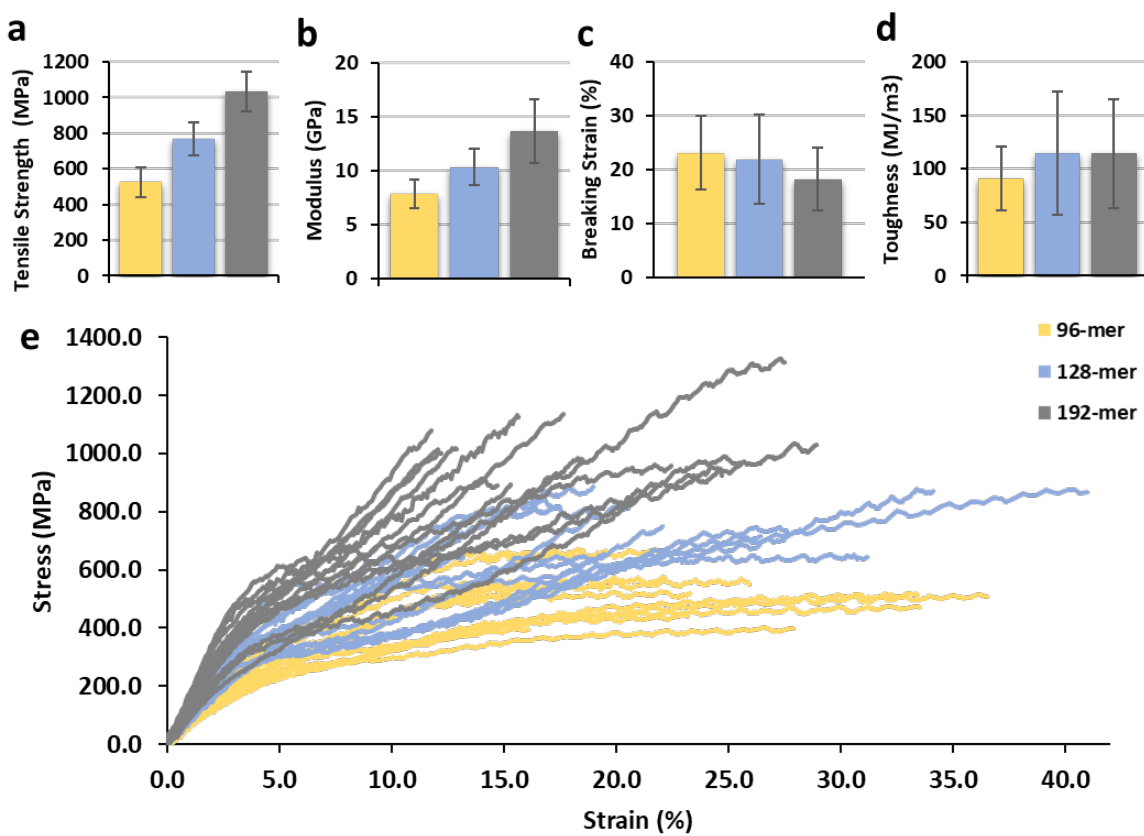
88 To facilitate microbial production of highly repetitive, SI-fused material proteins, we
89 developed a standardized DNA assembly strategy, termed SI-Bricks (Supplementary Note 1 and
90 Figure 1). The SI-Bricks strategy allows for rapid genetic swapping of the core components of
91 the devised SI-mediated ligation system (e.g. N-inteins, material proteins, C-inteins, and fusion
92 domains/purification tags) in addition to common standardized biological parts (e.g. promoters,
93 ribosomal binding sites, replication origins, and selection markers), all through simple restriction
94 enzyme digestion/ligations. With SI-Bricks, starting from a single codon-optimized repeat unit
95 (1-mer) of the *N. clavipes* dragline spidroin MaSp1, we assembled 64-mer and 96-mer spidroin
96 DNA sequences by iterative end-to-end restriction digestion/ligation. The spidroin sequences
97 were then genetically combined with codon-optimized SI DNA sequences and expression parts
98 (Supplementary Figure 2). The resulting SI-fused spidroins (^N64, 64^C, ^N96, and 96^C) were
99 individually expressed in an *E. coli* host with ^{glycyl}tRNA levels engineered to meet the demands
100 of the most frequently used glycine codons in the spidroin sequences (Methods). Following our
101 optimized fermentation conditions (Methods), typical titer of the SI-fused spidroins was nearly 2

102 g/L from glucose minimal medium with tryptone supplementation after four hours of production
103 (Supplementary Figure 3).

104 Spidroin inter- and intramolecular interactions are highly sensitive to salt and pH, even in
105 the presence of 8 M urea, and we expected that unwanted spidroin interactions would lower SI
106 ligation efficiency. Thus, to test optimum conditions for ligation of SI-fused spidroins, 8 M urea
107 extracts of *E. coli* expressing ⁶⁴N or ^C64 were mixed at several salt concentrations, temperatures,
108 and pH values (Extended Data Figure 1). Under all tested conditions, SI-mediated spidroin
109 ligation is both rapid and robust, with the highest ligation yields observed at 37 °C, 300 mM
110 NaCl, pH 7. Thus, for all subsequent ligations, these conditions were maintained, giving ligation
111 yields of 68% and 62% for 128-mer and 192-mer spidroin, respectively (Extended Figure Data
112 Figure 2). Ligation products were separated from most cellular proteins by selective precipitation
113 with ammonium sulfate and further separated from unreacted 64-mer or 96-mer by size
114 exclusion chromatography (SEC) for a final product purity ≥90% (Supplementary Fig. 4). As a
115 standard for mechanical properties, a 96-mer spidroin with no SIs was also expressed and
116 purified following identical procedures. All purified proteins were lyophilized and dissolved in
117 hexafluorisopropanol (HFIP) to yield 14% w/v spinning dopes which were wet-spun into solid
118 fibers by extrusion into a 95% methanol bath followed by immediate post-spin drawing.

119 Mechanical testing of post-drawn fibers revealed significant, nearly two-fold increases in
120 both tensile strength (from 525 ± 83 MPa to 1031 ± 111 MPa, $P < 0.0001$, $n=14$) and modulus
121 (from 7.8 ± 1.3 GPa to 13.7 ± 3.0 GPa, $P < 0.0001$, $n=14$) between 96-mer and 192-mer fibers
122 (Fig. 2a,b). Average toughness also increased slightly (25%), while average breaking strain
123 decreased slightly (22%), though neither change is statistically significant due to large fiber to
124 fiber variations (Fig. 2c, d). For both strength and modulus, 128-mer fibers showed performance

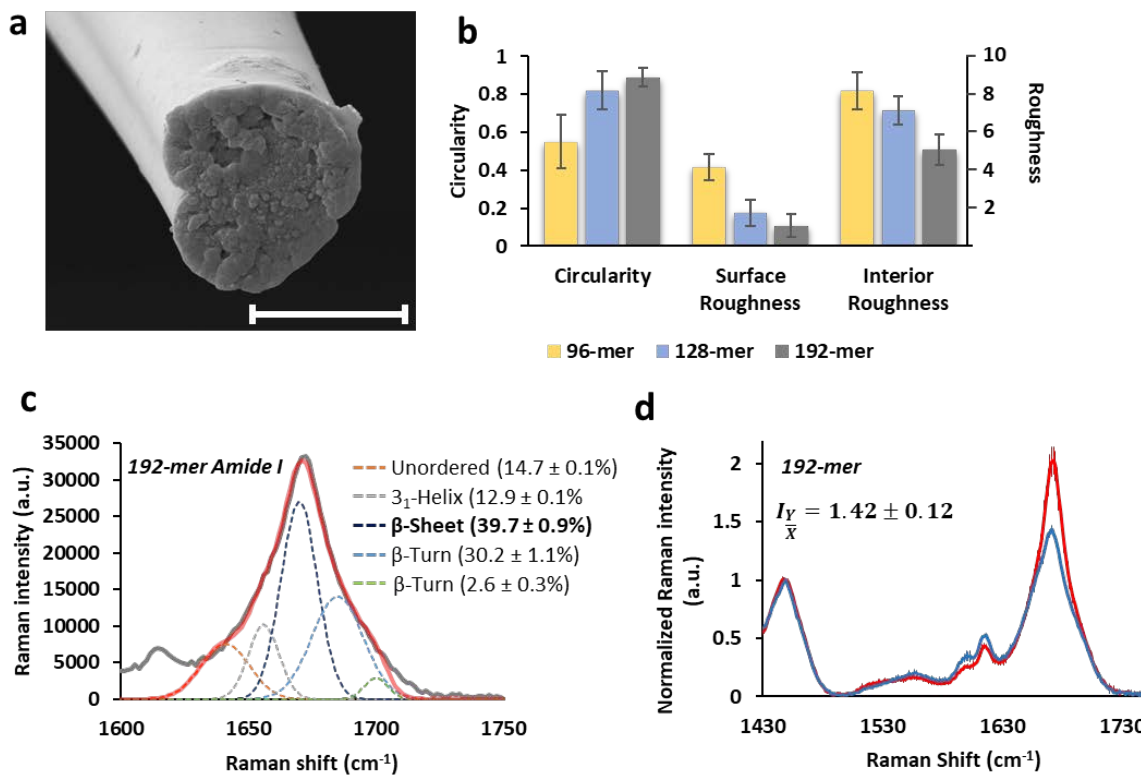
125 intermediate to 96- and 192-mer fibers. Together, these results strongly suggest that there
 126 remains a positive correlation between spidroin size and fiber strength and modulus up to a MW
 127 of at least 556 kDa. Most significantly, these results demonstrate that fibers spun from a
 128 microbially synthesized 192-mer *N. clavipes* dragline spidroin have mechanical properties
 129 equivalent to natural *N. clavipes* dragline silk (i.e., $\sigma = 993 \pm 140$ GPa, $E = 14.0 \pm 4.0$ GPa, $U_T =$
 130 111.2 ± 30 MJ/m³, $\epsilon = 16.3 \pm 3.8\%$, Extended Data Table 1).^{6,11,12,13}



131
 132 **Figure 2. Mechanical properties of synthetic silk fibers from high MW spidroins.** (a) Ultimate
 133 tensile strength, (b) elastic modulus, (c) breaking strain, and (d) toughness of 96-mer, 128-mer,
 134 and 192-mer fibers. All properties are calculated from stress-strain curves of 14 fibers for each
 135 MW. Error bars represent standard deviations, n = 14. (d) Compiled stress-strain curves for all
 136 fibers tested.

137

138 To gain insight into the origins of the exceptional strength and toughness of 192-mer
139 fibers, we examined fiber physical characteristics at both micro and molecular scales. At the
140 micro scale, light microscopy images confirmed that our fibers have consistent diameters along
141 the fiber axes and that diameters do not vary significantly with MW ($P = 0.1389$, unpaired t test,
142 Extended Data Table 1, Supplementary Fig. 5). Fiber diameters are also similar to those of
143 natural dragline fibers, which have been reported to range from 1-8 μm (Supplementary Fig.
144 5).^{12,11,14} Scanning electron microscopy (SEM) micrographs showed a distinct trend of
145 decreasing surface roughness as well as fewer interior defects with increasing MW (Extended
146 Fig. 3-5). To quantify this trend, fiber exterior and interior roughness were scored on a scale of
147 0-10, and mean roughness from six micrographs for each spidroin MW were calculated (Fig. 3b;
148 Supplementary Table 7). By this metric, surface roughness decreased 74% and interior roughness
149 decreased 39% between 96-mer and 192-mer fibers. Meanwhile, a trend of increased circularity
150 with increasing MW is also apparent from the SEM micrographs, with 96-mer fibers exhibiting
151 variations of a tri-lobed structure and 192-mer fibers exhibiting a mostly compact, nearly circular
152 morphology. The average circularity values for 192- and 96-mer fibers were $0.89 (\pm 0.05)$ and
153 $0.55 (\pm 0.14)$, with a perfect circle giving a value of 1 (see Methods for calculation) (Fig. 3b;
154 Supplementary Table 7).



155
156 **Figure 3. Fiber characteristics at micro and molecular scales. (a)** Representative SEM
157 micrograph of a 192-mer fiber showing nearly circular cross-section, with smooth surface and
158 dense, relatively smooth interior morphology similar to natural dragline fibers. Scale bar is 5
159 μm . **(b)** Quantification of fiber circularity, surface roughness and interior roughness, showing
160 general trend of increasing circularity and decreasing roughness with increased fiber MW.
161 Measures are from micrographs presented in Extended Data Figure 3-5. **(c)** Representative
162 amide I band deconvolution and secondary structure quantification for 192-mer fibers showing
163 β -sheet content similar to natural dragline fibers. **(d)** Amide I Raman spectra for 192-mer fibers
164 oriented parallel (blue lines) or perpendicular (red lines) to the direction of laser polarization.
165 As expected for anisotropic fibers with axial β -sheet crystal alignment, Amide I peak intensity

166 increases when fibers are oriented perpendicular to laser polarization (Supplementary Figure
167 6). Peak intensity ratio at 1670 cm⁻¹ (I_Y) is presented as an inset.

168

169 To further investigate fiber characteristics at the molecular scale, the 192-mer fibers were
170 analyzed by polarized Raman microspectroscopy. Deconvolution of the amide I band (1630-
171 1730 cm⁻¹) of Raman spectra confirm a high percentage ($39.7 \pm 0.9\%$) of β -sheet content in the
172 192-mer fibers (Fig. 3c), which agrees closely with β -sheet content ($37 \pm 3\%$) previously
173 reported for natural *N. clavipes* dragline fibers as determined by both FTIR and polarized
174 Raman.¹⁵ Meanwhile, several studies have established that dragline fibers exhibit a high degree
175 of chain alignment in the axial direction, with β -sheet crystals oriented parallel to the fiber axis—
176 an important contributing factor to the exceptional tensile strength of dragline fibers.^{16,17} Here,
177 the β -sheet alignment along the fiber axis was measured by comparing the amide I β -sheet
178 component (1670 cm⁻¹ peak intensities) between spectra acquired from fibers oriented both
179 parallel (X-axis) and perpendicular (Y-axis) to the direction of laser polarization (Supplementary
180 Fig. 6). The 192-mer fibers exhibited a peak intensity ratio (I_Y) of 1.42 ± 0.12 , which agrees
181 closely to ratios previously reported for natural *N. clavipes* dragline fibers (1.59).¹⁸ Overall, the
182 β -sheet content and alignment observed here confirm that the synthetic 192-mer fibers are
183 capable of recapitulating the structural characteristics of natural spider silk, which likely
184 contributes to its observed mechanical performance.

185 Taken together, the synthetic silk fibers produced from our process not only display the
186 key mechanical properties of natural silk but also characteristics including microscale
187 morphology, β -sheet content, and axial alignment of β -sheet crystals. The observed relationship
188 between spidroin MW and fiber strength suggest that spidroins larger than our 192-mer may

189 yield synthetic fibers even stronger than natural dragline silks. Additionally, integration of our
190 biosynthetic process with recent advances in biomimetic spinning could further improve fiber
191 performance and process simplification.

192 The fibers produced by this approach may accelerate the development of burgeoning
193 markets that specifically demand high strength silk fibers, such as projectile protection in defense
194 sectors, high strength lightweight cables and ropes in aerospace sectors, or high strength,
195 monofilament, thin fibers ($\leq 10 \mu\text{m}$) for medical sutures. These applications are especially likely
196 with further improvements in process yield. Moreover, the platform developed here can be easily
197 expanded to other large and highly repetitive material proteins (e.g. collagens, elastins, sucker
198 ring teeth proteins) for their microbial production from cheap and renewable feedstock.

199

200

201 **Full Methods** and any associated references are available in the online version of the paper at...

202

203 **Acknowledgements** We would like to thank Tavis Reed and Beryl Mpamo for their assistance
204 with protein production; Srikanth Singamaneni, Sirimuvva Tadepalli, and Rohit Gupta for
205 assistance with Raman microspectroscopy; and Xiaoxia Xia for suggestions on fiber spinning.
206 We thank the Tianjin Institute of Industrial Biotechnology for providing the synthetic DNA
207 sequence of *N. clavipes* MaSp1. This work was supported by a Young Investigator Program from
208 AFOSR (FA95501510174 to FZ) and an Early Career Faculty grant from NASA's Space
209 Technology Research Grants Program (NNX15AU45G to FZ).

210

211 **Author Contributions** F.Z. conceived the project. C.H.B. performed sequence/host
212 optimizations, protein production, fiber spinning, and fiber characterizations. B.D. performed
213 genetic assembly, protein production, and protein purification. C.S. performed SEM imaging.
214 W.B. provided the original 1-mer sequence and production advice. P.L. and H.F. performed
215 protein production. W.H. and D.K. provided training and advice in fiber spinning and
216 characterization. J.G. provided advice and data analysis. C.B., C.S., and F.Z. prepared the
217 manuscript.

218

219 **Author Information** The authors declare no competing financial interests. Correspondence and
220 requests for materials should be addressed to F.Z. (fzhang@seas.wustl.edu).
221

222 **METHODS**

223 **Strains and growth conditions.** *E. coli* NEB 10-beta (NEB10 β) was used for all plasmid
224 cloning and protein production. For all cloning, *E. coli* strains were cultured in Terrific Broth
225 (TB) containing 24 g/L yeast extract, 20 g/L tryptone, 0.4% glycerol, 17 mM KH₂PO₄, and 72
226 mM K₂HPO₄ at 37°C with appropriate antibiotics (50 µg/mL kanamycin and 30 µg/mL
227 chloramphenicol). M9 glucose medium with tryptone supplement (2% Glucose, 1x M9 Salts, 75
228 mM MOPS pH 7.4, 12 g/L tryptone, 5 mM Citrate, 2 mM MgSO₄·7H₂O, 100 µM FeSO₄·7H₂O,
229 100 µM CaCl₂·2H₂O, 3 µM thiamine, 1x micronutrients [40 µM ZnSO₄·7H₂O, 20 µM
230 CuSO₄·5H₂O, 10 µM MnCl₂·4H₂O, 4 µM H₃BO₃, 0.4 µM (NH₄)₆Mo₇O₂₄·4H₂O, and 0.3 µM
231 CoCl₂·6H₂O]) was used for protein production in bioreactors.

232 **Chemicals and reagents.** Unless otherwise noted, all chemicals and reagents were
233 obtained from Sigma-Aldrich (St. Louis, MO, USA). Plasmid purification and gel extraction kits

234 were purchased from iNtRON Biotechnology (Lynnwood, WA, USA). FastDigest restriction
235 enzymes and T4 DNA ligase were purchased from ThermoFisher Scientific (Waltham, MA,
236 USA) and used for all digestions and ligations following the manufacturer's suggested protocols.

237 **Genetic assembly of 64- and 96-mer spidroins.** The repeated spidroin DNA sequences
238 were constructed using a method modified from previous work (Supplementary Figure 2). The
239 coding sequence of 1-mer *N. clavipes* MaSp1 was obtained from Tianjin Institute of Industrial
240 Biotechnology (Supplementary Table 1) and chemically synthesized by Integrated DNA
241 Technologies (San Jose, CA, USA). This DNA sequence was flanked on the 5' end by restriction
242 sites 5'-KpnI/NheI-3' and on the 3' end by restriction sites 5'-SpeI/Kpn2I-3'. The sequence was
243 inserted between restriction site KpnI/Kpn2I of a medium copy (pBBR1 replication origin)
244 chloramphenicol resistance (CmR) expression vector, resulting in plasmid p1. To begin the
245 iterative DNA assembly, plasmid p1 was linearized by digestion with NheI and ligated with a
246 second 1-mer sequence digested by NheI/SpeI. The ligation was transformed to NEB10 β for
247 amplification, yielding plasmid p2 containing 2-mer spidroin. The same procedure was repeated
248 for p2, with insertion of a linearized 2-mer sequence, to yield plasmid p4. The process was
249 repeated until p64 (32-mer + 32-mer) and p96 (64-mer + 32-mer) were obtained. Because the
250 annealing of the NheI and SpeI complementary overhangs from joining fragments does not
251 produce a new restriction site, digestion with NheI was used to confirm the proper orientation of
252 the insert at each step based on fragment sizes.

253 **Construction and sequence optimization of silk-SI-fusion proteins.** N- and C-terminal
254 SI amino acid sequences (Cfa^N and Cfa^C, respectively) were obtained from a recent publication.
255 SI coding sequences were optimized for *E. coli* expression along with 5'UTR and RBS sequences
256 using a combination of computational approaches. Specifically, using the Gene Designer 2.0

257 (ATUM) software, a variable Cfa^C coding sequence was flanked on the 3' end by invariable 5'-
258 KpnI/NheI-3' restrictions sites and repetitive silk sequences, and on the 5' end by an invariable
259 RBS/5'-UTR (5'-ATCAGCAGGACGCCTGACCGAATTCAAAAGATCTTTAAGAAGGA
260 GATATACAT-3'), including the 5'-EcoRI/BglII-3' restriction sites, and short peptide coding
261 sequence 5'-ATGGCTAACAGACTAAA-3' (for increased translation initiation rate, as described
262 previously; Supplementary Table 1). Considering these flanking invariable sequences, the
263 variable Cfa^C sequence was optimized using a modified *E. coli* codon usage table and giving
264 extra weight to 5' mRNA structure minimization during sequence optimization. The resulting
265 sequence (Supplementary Table 1) containing the 5'UTR and Cfa^C was synthesized as a gblock
266 fragment by Integrated DNA Technologies and was inserted 5' of the 64-mer or 96-mer
267 sequences by digestion/ligation with BglII/KpnI to yield plasmids p^C64x and p^C96x, which
268 encode fusion proteins ^C64 and ^C96, respectively (Supplementary Table 2). Similarly, the
269 variable Cfa^N sequence was flanked on the 5' end by invariable 5'-SpeI/Kpn2I-3' restrictions sites
270 and on the 3' end by an invariable 5'-BamHI/XhoI-3' site and subjected to the same optimization
271 process as Cfa^C. The resulting Cfa^N sequence was synthesized and inserted 3' of the 64-mer and
272 96-mer sequences by digestion/ligation with Kpn2I/BamHI to yield plasmids p64^N and p96^N,
273 which encode fusion proteins 64^N and 96^N, respectively. The resulting constructs allow for easy
274 swapping of any Int^C of interest by digestion with BglII/KpnI and any Int^N of interest by
275 digestion with Kpn2I/BamHI, while the presence of NheI/SpeI sites allows for iterative genetic
276 assembly of any large or other repetitive material proteins of interest (Supplementary Figure 1).

277 **Upregulation of GlyV tRNA production.** In addition to sequence optimizations, cellular
278 ^{glycyl}tRNA levels were also upregulated to meet the high demands on ^{glycyl}tRNA posed by
279 spidroin overexpression. The glyV tRNA coding sequence and its native promoter were PCR-

280 amplified from the NEB10 β genomic DNA (Supplementary Table 1) and cloned between
281 AatII/XhoI sites of a medium copy vector carrying p15A replication origin and Kanamycin
282 resistance (Kan^R), yielding plasmid pGlyV (Supplementary Table 2). For all spidroin expression,
283 pGlyV was co-transformed with the spidroin plasmid.

284 **Shake flask cultures.** For initial ligation tests as shown in Supplementary Figures 2 & 4,
285 protein production was carried out in shake flasks. Transformants were cultured overnight in 50
286 mL TB medium at 37 °C on an orbital shaker. Overnight 50 mL cultures were then inoculated
287 into 500 mL fresh TB medium in Erlenmeyer flasks at an initial OD₆₀₀ = 0.08. Cultures were
288 grown at 37°C with orbital shaking to OD₆₀₀ = 6, then induced by addition of 1 mM IPTG and
289 cultured for an additional 6 hours at 30°C with orbital shaking.

290 **Bioproduction in fed-batch bioreactors.** All spidroins were finally produced in 2 L fed-
291 batch bioreactors (Bioflo120, Eppendorf). Transformants were cultured overnight in 50 mL TB
292 medium at 37°C on an orbital shaker. The overnight cultures were then inoculated into 1 L
293 glucose M9 medium with tryptone supplement with an initial OD₆₀₀ = 0.08. After overnight
294 incubation at 37°C with orbital shaking, 1 L cultures were pelleted by centrifugation at 4500 x g
295 for 10 min and resuspended in 300 mL sterile resuspension medium (250 mM MOPS pH 7.4,
296 2.5% glucose, 60 g/L tryptone, 25 mM citrate, 10 mM MgSO₄, 500 μ M FeSO₄·7H₂O, 15 μ M
297 thiamine, 5x micronutrients). The resuspended cultures were then added to an autoclaved 2 L
298 Bioflo120 heat-blanketed bioreactor containing 1.2 L water and 1.15x M9 salts. Sterile
299 CaCl₂·2H₂O was added to a final concentration of 100 μ M. Antifoam 204 was added as needed to
300 minimize foaming (approximately 0.01%). Agitation and air flow was regulated to maintain
301 approximately 70% dissolved oxygen (DO). After consumption of the initial 0.5% glucose (as
302 judged by Δ DO), a sterile substrate feed (20% glucose, 48 g/L tryptone, and 10 g/L

303 $\text{MgSO}_4 \cdot 7\text{H}_2\text{O}$) was initiated to maintain a linear growth rate. Reactors were induced at $\text{OD}_{600} =$
304 80 by addition of 1 mM IPTG and culture temperature was reduced to 30°C. Cultures were
305 collected four hours after induction. Titers were estimated from densitometric analysis of
306 Coomassie Blue-stained SDS-PAGE gels (Supplementary Figure 3).

307 **Protein ligation.** Cell cultures were pelleted by centrifugation at 4500 x g for 30 min.
308 Pellets from complimentary SI-fused spidroins (e.g. 96^N and ^C96 or 64^N and ^C64) were combined
309 at a 1:1 reactant ratio based on densitometric analysis of Coomassie Blue-stained SDS-PAGE
310 gels. Mixed pellets were resuspended in sonication buffer (300 mM NaCl, 20 mM MOPS pH
311 7.4, 2 mM TCEP, 1 mM PMSF) and sonicated using a QSonica Q700 sonicator (Qsonica,
312 Newton, CT, USA) for 10 min. Sonicated resuspensions were pelleted by centrifugation at
313 25,000 x g for 30 min to remove supernatants. Pellets were resuspended in ligation buffer (8 M
314 urea, 20 mM MOPS pH 7.4, 300 mM NaCl, and 2 mM TCEP) and stirred at 37°C for 24 h to
315 dissolve SI-fused spidroins and allow maximal ligation yield. The mixtures were then
316 centrifuged at 25,000 x g for 1 h to remove cell debris and undissolved proteins.

317 **Protein purification.** The purification protocol was modified from previous methods.
318 Specifically, ligated spidroins in ligation buffer were acidified with acetic acid to pH 4.0.
319 Ammonium sulfate was then added to a final concentration of 1.2 M. The mixture was then
320 centrifuged at 40,000 x g for 30 min. The pellet was discarded, and additional ammonia sulfate
321 was added to the supernatant to a final concentration of 2.3 M. After stirring for 1 h, the mixture
322 was centrifuged again at 40,000 x g for 15 min. The supernatant was discarded, and the pellet
323 was resuspended in SEC buffer (8 M urea, 10 mM ammonium bicarbonate pH 10) for further
324 purification by size-exclusion chromatography. SEC purifications were performed on an AKTA
325 Pure Chromatography System (GE Healthcare Life Sciences) using a HiPrep 16/60 Sephadex S-

326 500 HR column (for 128-mer and 192-mer) or a HiPrep 16/60 Sephadryl S-400 HR column (for
327 96-mer). Proteins were separated using an isocratic elution with SEC buffer at a flow rate of 0.5
328 mL/min. Fractions containing greater than 90% ligation product, as determined by SDS-PAGE
329 gel densitometry, were collected. SEC-purified fractions were combined and dialyzed in 10K
330 MWCO SnakeSkin dialysis tubing (ThermoFisher Scientific) against 10 mM acetic acid aqueous
331 solution. The dialyzed samples were then lyophilized.

332 **Ligation kinetics analysis.** For kinetics analysis, 64-mer protein concentrations in crude
333 lysates were estimated by densitometric analysis of Coomassie Blue-stained SDS-PAGE gels.
334 Based on estimated concentrations, fully sonicated resuspensions of ^{64}C and $^{\text{N}}\text{64}$ in ligation
335 buffer were combined to give final concentrations of 100 μM for both ^{64}C and $^{\text{N}}\text{64}$ in a final
336 volume of 500 μL . Combined resuspensions were pelleted by centrifugation, and pellets were
337 resuspended in 500 μL of desired test buffer pre-incubated at the desired test temperature.
338 Reactions were quenched by transferring 5 μL of reaction to 95 μL of Laemmli sample buffer
339 preheated to 100°C and continuing boiling for 10 min.

340 **SDS-PAGE and densitometric analysis.** All SDS-PAGE gels were 1 mm thick,
341 discontinuous with 3% stacking gel, and hand cast at the indicated percentages. Samples were
342 prepared at 1 mg/mL or 5 μM total protein in Laemmli sample buffer (2% SDS, 10% glycerol,
343 60 mM Tris pH 6.8, 0.01% bromophenol blue, 100 μM DTT). Gels were run on Mini-
344 PROTEAN Tetra Cells (Bio-Rad) in 1x Tris-glycine SDS buffer (25 mM Tris base, 250 mM
345 glycine, 0.1% SDS), until just before the dye front exited the gel. Gels were stained in
346 Coomassie Blue solution (50% methanol, 10% acetic acid, 1 g/L Coomassie Brilliant Blue) for a
347 minimum of one hour at room temperature with gentle agitation and destained in Coomassie
348 Blue destain buffer (40% methanol, 10% acetic acid) for a minimum of 1 hour. Gels were

349 imaged on an Azure c600 Imager (Azure Biosystems). All densitometry analysis was performed
350 with the AzureSpot Analysis Software (Azure Biosystems). Images were background subtracted
351 with an automatic valley-to-valley baseline detection. Protein band intensities were integrated by
352 the software. Ligation yield was calculated as the intensity of the product band over the sum of
353 both reactant and product band intensities. Spidroin titer was calculated as the intensity of the
354 spidroin band over the sum of all band intensities multiplied by 150 mg/L/OD₆₀₀ and cell density
355 at OD₆₀₀. (150 mg/L/OD₆₀₀ is the typical total protein titer in DH10 β *E. coli* cells).

356 **Fiber spinning and mechanical testing.** Fiber spinning and mechanical testing were
357 performed following a protocol modified from previous methods. Lyophilized spidroin powders
358 were dissolved in hexafluorisopropanol (HFIP) to 14% w/v. This protein dope was loaded to a
359 100 μ L Hamilton gastight syringe (Hamilton Robotics) fitted with a 23s gauge (116 μ m inner
360 diameter, 1.71 inch length) needle. The syringe was fitted to a Harvard Apparatus Pump 11 Elite
361 syringe pump (Harvard Apparatus), and the dope was extruded into a 95% methanol bath at 5
362 μ L/min (approximately 0.5 m fiber/min). Extruded fibers were then transferred to a 75%
363 methanol bath and carefully extended at approximately 1 cm/s to the maximum draw ratio
364 without fiber fracture (6x for 96-mer fibers, 9x for 128- and 192-mer fibers). Extended fibers
365 were removed from the bath and held under tension until visibly dry. Segments of post-drawn
366 fibers (20 mm) were carefully laid exactly vertical across a 5 mm square opening cut into a 20
367 mm square piece of cardstock and fixed with adhesive tape at both ends of the opening.
368 Diameters of mounted fibers were then measured by light microscopy, averaging measurements
369 at three points along the fiber axis. Mechanical properties were measured by axial pull tests on
370 an MTS Criterion Model 41 universal test frame fitted with a 1N load cell (MTS Systems
371 Corporation). Cardstock holders were mounted between two opposing spring-loaded grips, and

372 the supporting edges were carefully cut. Pull tests were conducted with a constant crosshead
373 speed of 10 mm/min. Stress-strain curves were recorded by the MTS TW Elite test suite at a
374 sampling rate of 50 Hz. Fiber breaks were recorded when a 90% drop from peak stress was
375 detected. All mechanical properties were automatically calculated by the MTS TW Elite test
376 suite. Ultimate tensile strength was calculated as the maximum measured load over the initial
377 fiber cross-sectional area ($A = \pi r^2$), as determined from measured initial diameters. Modulus
378 was calculated as the slope of a linear least squares fit to the stress/strain data of the initial elastic
379 region. Toughness was calculated as the area under the total stress/strain curve divided by the
380 initial fiber volume ($V = \pi r^2 h$) as calculated from measured initial fiber diameters and set initial
381 gage length of 5 mm. For each protein, a total of 14 fibers were measured in this manner.

382 **Light microscopy.** Fiber diameters were measured using images acquired with a Zeiss
383 Axio Observer ZI Inverted Microscope equipped with a 20x objective lens and the Axiovision
384 LE software (Zeiss). For morphological analysis and further confirmation of fiber diameters,
385 additional images were acquired with a Nikon Eclipse TiE Inverted Microscope equipped with a
386 60x objective and analyzed using the Nis-Elements software (Nikon).

387 **Scanning Electron Microscopy.** Following tensile tests, silk fibers were mounted onto a
388 sample holder using conductive tape. The sample holder was sputter coated with a 10 nm gold
389 layer using a Leica EM ACE600 high vacuum sputter coater (Leica Microsystems). Fibers were
390 imaged using a Nova NanoSEM 230 Field Emission Scanning Electron Microscope (FEI) at
391 an accelerating voltage of 7-10 kV. Fiber circularity was calculated from cross-sectional areas
392 and perimeters as $4\pi(\frac{area}{perimeter^2})$, where a perfect circle gives a value of 1.

393 **Polarized Raman microspectroscopy.** Silk fibers were carefully fixed to glass
394 microscope slides with microscale markings to ensure that spectra were acquired at the same

location before and after stage rotation. Raman spectra were acquired with a Renishaw RM1000 InVia Confocal Raman Spectrometer (Renishaw) coupled to a Leica DM LM microscope with rotating stage (Leica Microsystems). Silk fibers were initially oriented along the x-axis as depicted in Supplementary Figure 9. Fibers were irradiated at a fixed point with the 514 nm line of an argon laser with polarization fixed along the x-axis and focused through a 50x objective (NA = 0.75). Spectra were recorded from 1150-1750 cm⁻¹ with an 1800 lines/mm grating. For each acquisition, a total of 16 spectra were accumulated, each for 10 s. The stage was then rotated to orient fibers along the y-axis with the same laser polarization, and spectra were acquired a second time at the same fixed point. No signs of thermal degradation were apparent either visually or within recorded spectra. All recorded spectra were analyzed using the Fityk 0.9.8 software. Baselines were subtracted from all spectra using the built-in Fityk convex hull algorithm. For secondary structure determination, the amide I peak of y-axis oriented fibers was deconvolved into a set of five gaussian peaks centered at 1641, 1656, 1670, 1685, and 1700 cm⁻¹ for unordered, $\text{\textgreek{3}_1}$ -Helix, β -Sheet, β -Turn, and β -Turn components, respectively, as previously reported. Peak areas were integrated and percentages were calculated as the component peak area over the sum of all peak areas. Percentages were averaged from measurements of three fibers. For intensity ratio calculations, all spectra were normalized to the intensity of the 1450 cm⁻¹ peak, which arises from CH₂ bending and is insensitive to protein conformation. For each fiber, the normalized intensity at 1670 cm⁻¹ of the peak oriented along the Y-axis was divided by the normalized intensity of the peak oriented along the x-axis to give the intensity ratio (I_Y/I_X). This procedure was performed on a total of three separate fibers and calculated intensity ratios were averaged. Spectra were also averaged and presented in Figure 3d with standard deviations for each point along the spectra.

418

419 **Extended Data Table 1. Averaged mechanical properties for fibers spun from synthetic
420 spidroins compared to natural *N. clavipes* dragline fibers.**

Spidroin	MW. (kDa)	Tensile Strength (MPa) ¹	Young's Modulus (GPa) ¹	Toughness (MJ/m ³) ¹	Breaking Strain (%) ¹	Diamete r (μm) ¹	Source
Synthetic 96-mer	277	525 ± 83	7.8 ± 1.3	91 ± 30	23 ± 7	6.3 ± 0.7	Present study
Synthetic 128-mer	373	767 ± 92	10.3 ± 1.7	115 ± 58	22 ± 8	6.6 ± 0.9	Present study
Synthetic 192-mer	556	1031 ± 111	13.7 ± 3.0	114 ± 51	18 ± 6	5.7 ± 1.3	Present study
<i>Natural N. clavipes Dragline</i>	-	950 ± 381	12 ± 5.2	NA	16.9 ± 5.2	NA	Cunniff 1994 (Adapted from Zemlin, 1968)
<i>Natural N. clavipes Dragline</i>	-	972	12.7	NA	18.1	NA	Cunniff 1994 (Adapted from Zemlin, 1969)
<i>Natural N. clavipes Dragline</i>	-	875	10.9	NA	16.7	NA	Cunniff 1994 (Adapted from Zemlin, 1969)
<i>Natural N. clavipes Dragline</i>	-	1100	22	NA	9	3.7 ± 0.8	Cunniff, 1994
<i>Natural N. clavipes Dragline</i>	-	850	12.7	NA	20	4.2	Ko, 2001
<i>Natural N. clavipes Dragline</i>	-	1215 ± 233*	13.8 ± 3.6	111.2 ± 30	17.2 ± 3.5	NA	Swanson, 2006
<i>N. clavipes Dragline Average**</i>		993 ± 140	14.0 ± 4.0	111.2 ± 30	16.3 ± 3.8	3.7 ± 0.8	Combined

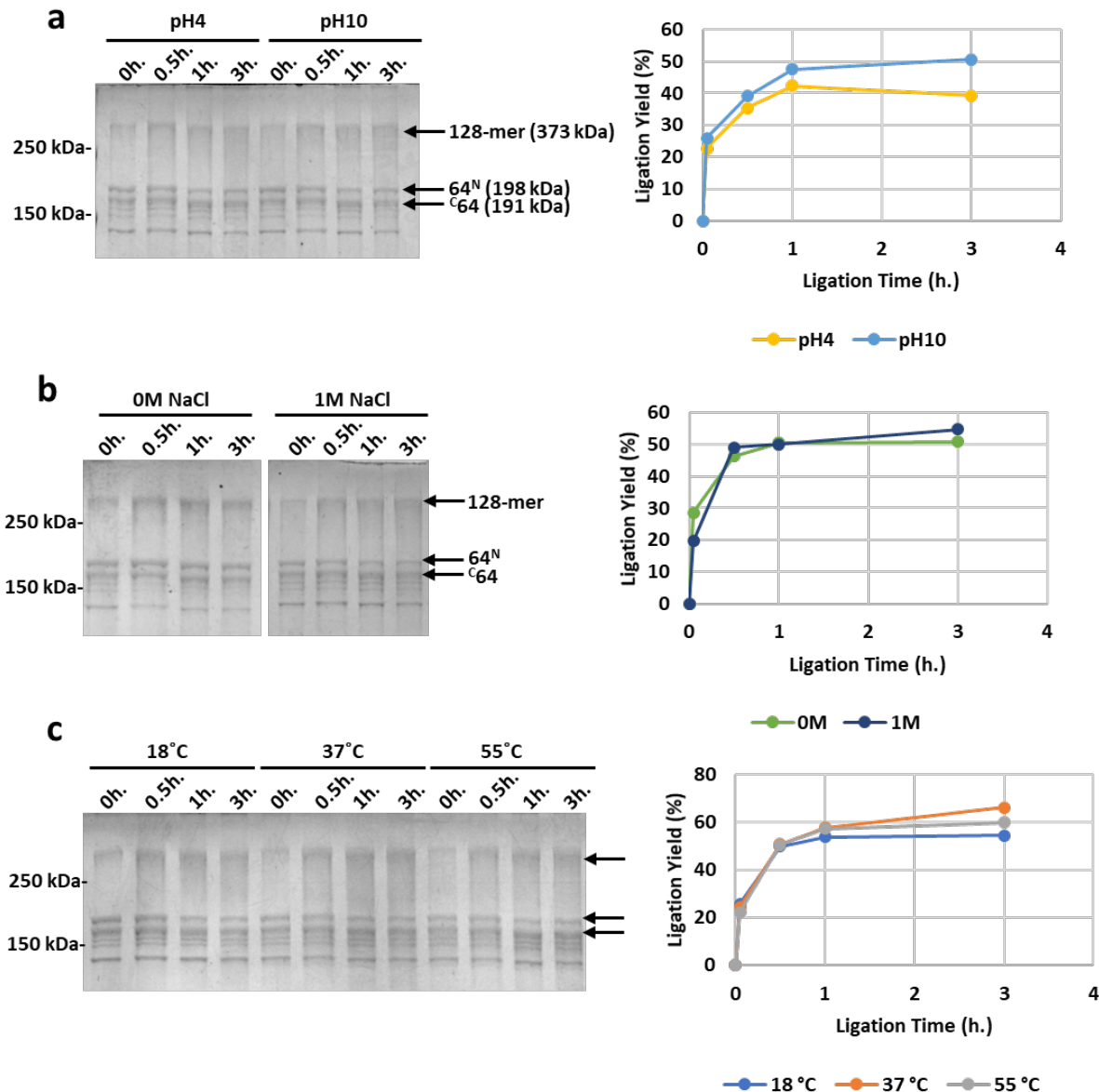
421 ¹ For all mechanical measurements, n = 14.

422 * Swanson et al. reported "true" stress values rather than the more commonly reported
423 "engineering stress" values. True stress calculates strength based on the final diameter of the
424 fiber assuming constant volume deformation, thus true stress values are expected to be
425 significantly higher than engineering stress values as calculated in the present study.

426 ** Averaged from the six sources compiled in this table.

427 NA: values could not be found in the referenced study.

428



431 **Extended Data Figure 1. Kinetics of SI-catalyzed ligation of spidroins.** SDS-PAGE (left) of
432 reaction mixtures containing 1:1 ratio of 64^N and $^{C}64$ in 8 M urea, 2mM TCEP at different pH (a)
433 pH4 = (300 mM NaCl, 10 mM ammonium acetate pH 4); pH10 = (300 mM NaCl, 10 mM
434 ammonium bicarbonate pH 10); different salt concentration (b) 0M = (0M NaCl, 10 mM MOPS
435 pH 7.4); 1M = (1M NaCl, 10 mM MOPS pH 7.4); and different temperature (c) all buffers =

436 (300 mM NaCl, 10mM MOPS pH 7.4). Black arrows indicate the expected size of product and
437 reactant bands. Ligation yields (right) were calculated as the area of the product band over the
438 sum of both reactant and product bands. Note, spidroins used in this experiment were produced
439 from shake flasks, which produce lower final titers than those from fed-batch bioreactors.

440

441

442

443

444

445

446

447

448

449

450

451

452

453

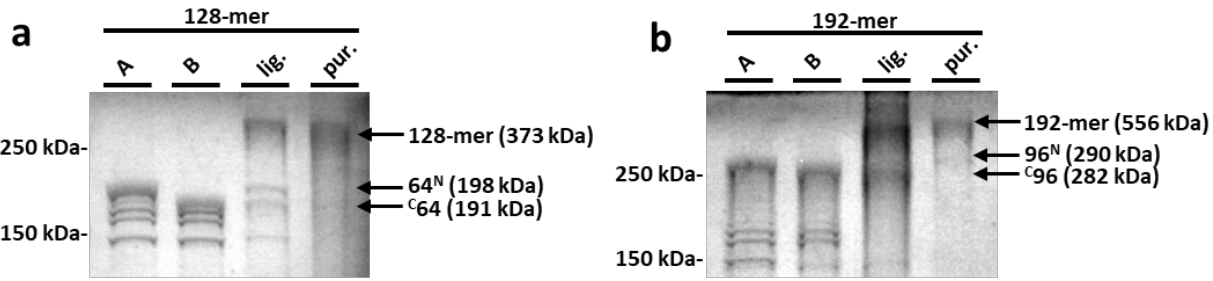
454

455

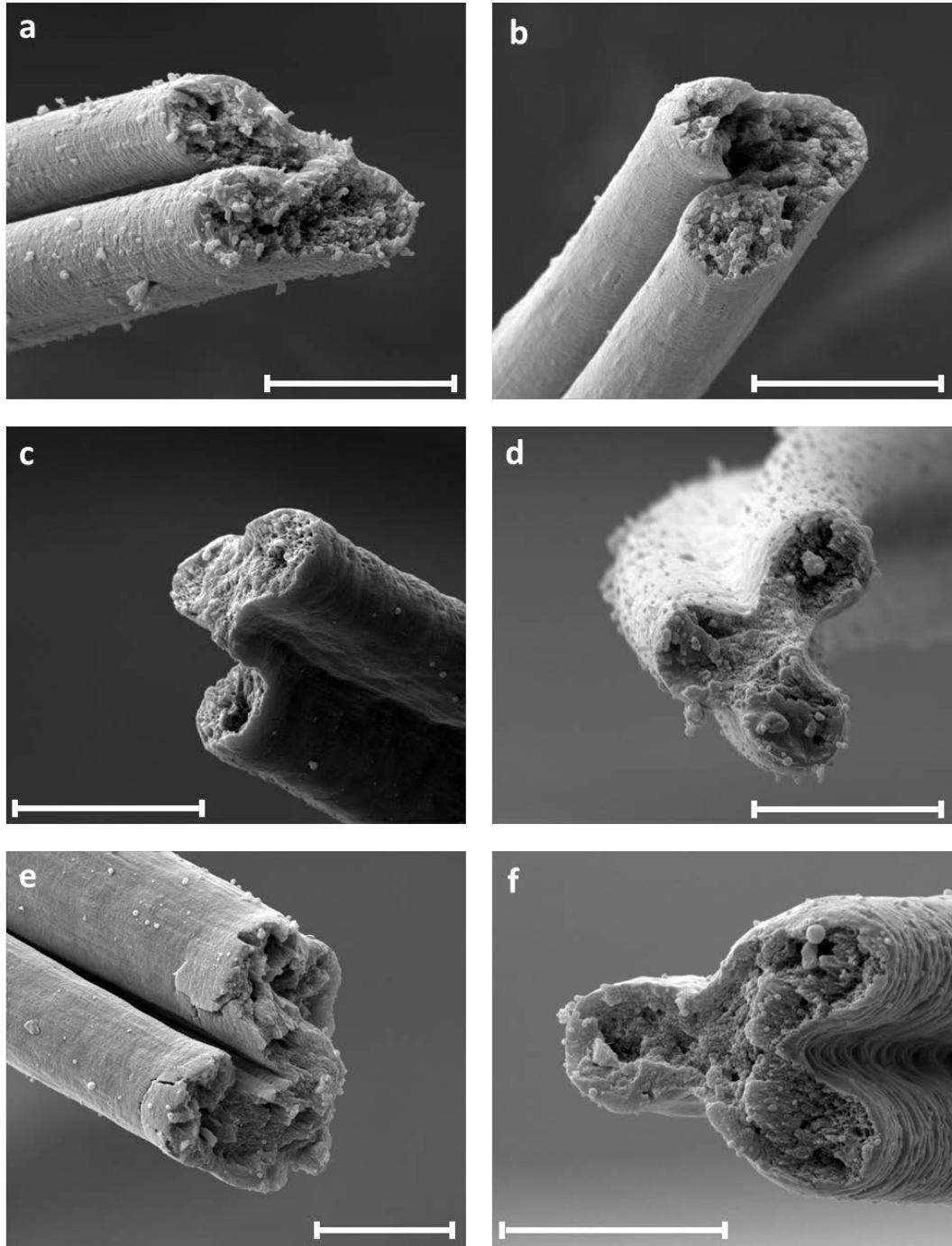
456

457

458



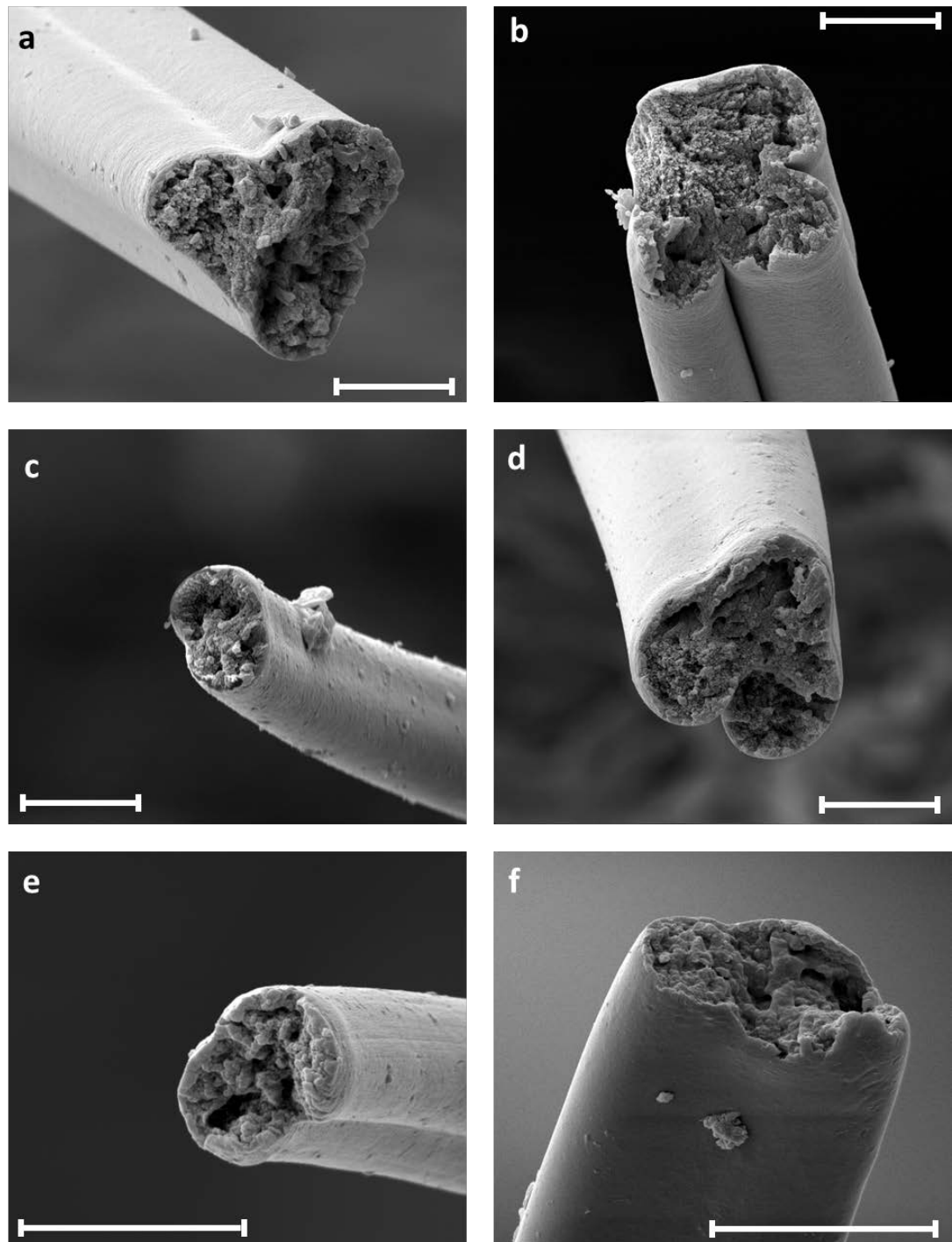
459
460 **Extended Data Figure 2. Ligation yields for 128-mer and 192-mer.** Coomassie Blue stained
461 SDS-PAGE gels for (a) 64^N + $c64$ ligation and (b) 96^N + $c96$ ligation. Lane 1, whole cells
462 expressing Cfa^N-fused spidroins (64^N or 96^N); lane 2, whole cells expressing Cfa^C-fused
463 spidroins ($c64$ or $c96$); lane 3, ligation products after selective ammonium sulfate precipitation;
464 lane 4, products after SEC purification.
465
466
467
468
469
470
471
472
473
474
475
476
477



478

479 **Extended Data Figure 3. Representative SEM micrographs of 96-mer fibers.** All samples
480 were taken after tensile tests. All scale bars are 5 μ m.

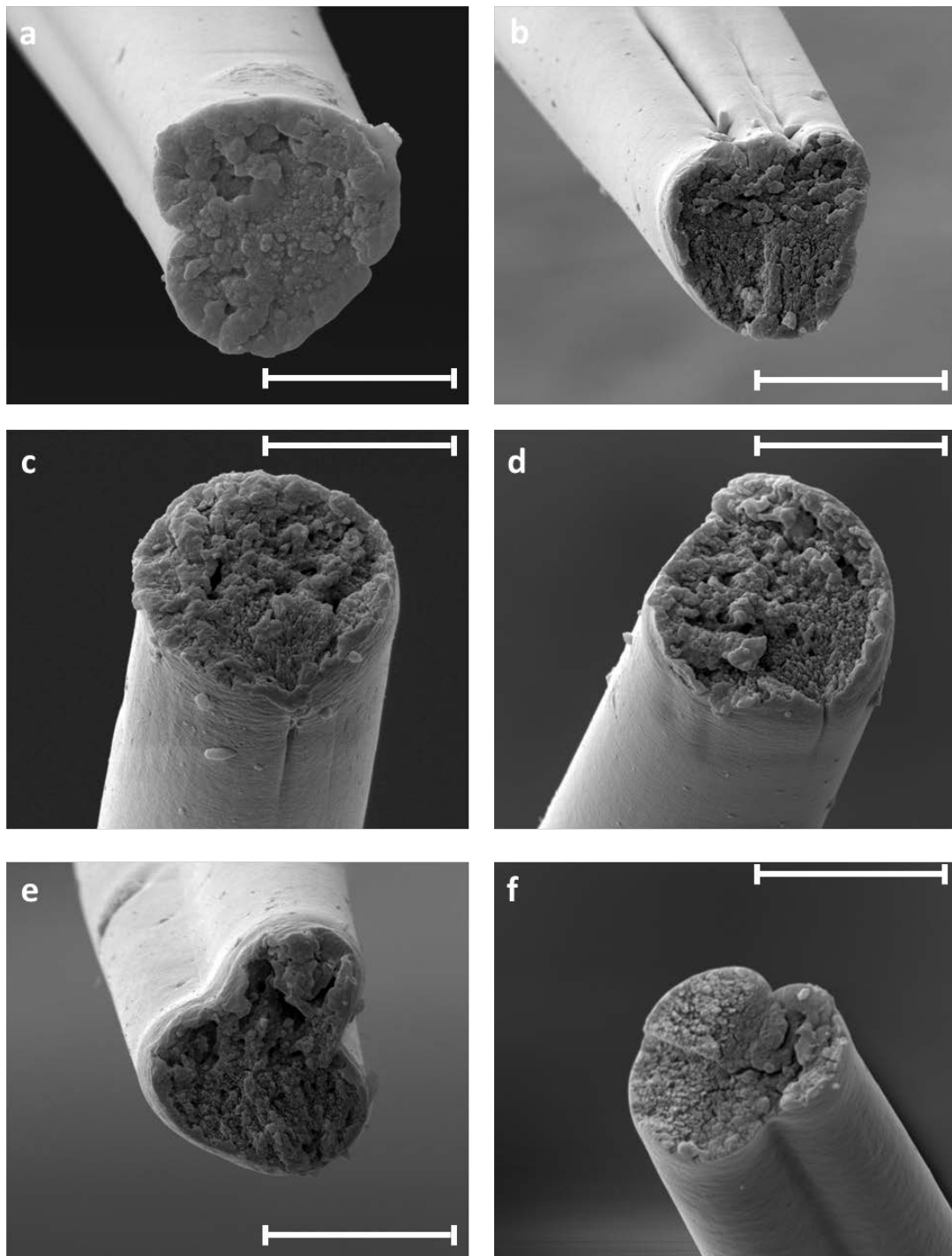
481



482

483 **Extended Data Figure 4. Representative SEM micrographs of 128-mer fibers.** All samples
484 were taken after tensile tests. All scale bars are 5 μ m.

485



486

487 **Extended Data Figure 5. Representative SEM micrographs of 192-mer fibers.** All samples
488 were taken after tensile tests. All scale bars are 5 μ m.

489

490

491 **REFERENCES**

- 492 1. Omenetto, F. G. & Kaplan, D. L. New Opportunities for an Ancient Material. *Science*.
493 **329**, 528–531 (2010).
- 494 2. Tokareva, O., Michalczechen-Lacerda, V. a., Rech, E. L. & Kaplan, D. L. Recombinant
495 DNA production of spider silk proteins. *Microb. Biotechnol.* **6**, 651–663 (2013).
- 496 3. Heidebrecht, A. & Scheibel, T. *Recombinant Production of Spider Silk Proteins. Advances*
497 *in Applied Microbiology* **82**, (Elsevier, 2013).
- 498 4. Teulé, F. *et al.* A protocol for the production of recombinant spider silk-like proteins for
499 artificial fiber spinning. *Nat. Protoc.* **4**, 341–55 (2009).
- 500 5. Xia, X.-X. *et al.* Native-sized recombinant spider silk protein produced in metabolically
501 engineered Escherichia coli results in a strong fiber. *Proc. Natl. Acad. Sci. U. S. A.* **107**,
502 14059–63 (2010).
- 503 6. Swanson, B. O., Blackledge, T. A., Summers, A. P. & Hayashi, C. Y. Spider Dragline
504 Silk: Correlated and Mosaic Evolution in High-Performance Biological Materials.
505 *Evolution (N. Y.)*. **60**, 2539 (2006).
- 506 7. Babb, P. L. *et al.* The Nephila clavipes genome highlights the diversity of spider silk
507 genes and their complex expression. *Nat. Genet.* **49**, 895–903 (2017).
- 508 8. Nunes, Ronald; Martin, John; Johnson, J. Influence of Molecular Weight and Molecular
509 Weight Distribution on Mechanical Properties of Polymers. *Polym. Eng. Sci.* **22**, 205–228
510 (1982).
- 511 9. Shah, N. H. & Muir, T. W. Inteins: Nature's Gift to Protein Chemists. *Chem. Sci.* **5**, 446–
512 461 (2014).
- 513 10. Stevens, A. J. *et al.* Design of a Split Intein with Exceptional Protein Splicing Activity. *J.*

- 514 *Am. Chem. Soc.* **138**, 2162–2165 (2016).
- 515 11. Zemlin, J. C. A study of the mechanical behavior of spider silks. *U.S. Army Natick Rep.*
516 *AD-684 333* 1–68 (1968).
- 517 12. Cunniff, P. & Fossey, S. Mechanical and thermal properties of dragline silk from the
518 spider *Nephila clavipes*. *Polym. ...* **5**, 401–410 (1994).
- 519 13. Ko, F. K. *et al.* Engineering Properties of Spider Silk. *Mater. Res. Soc. Symp. Proc.* **702**,
520 U1.4.1 (7 pages) (2001).
- 521 14. Prez-Rigueiro, J., Elices, M. & Llorca, C. V. Tensile properties of *Argiope trifasciata* drag
522 line silk obtained from the spider's web. *J. Appl. Polym. Sci.* **82**, 2245–2251 (2001).
- 523 15. Lefèvre, T., Rousseau, M. E. & Pézolet, M. Protein secondary structure and orientation in
524 silk as revealed by Raman spectromicroscopy. *Biophys. J.* **92**, 2885–2895 (2007).
- 525 16. Su, I. & Buehler, M. J. Nanomechanics of silk: the fundamentals of a strong, tough and
526 versatile material. *Nanotechnology* **27**, 302001 (2016).
- 527 17. Prince, J. T., McGrath, K. P., DiGirolamo, C. M. & Kaplan, D. L. Construction, cloning,
528 and expression of synthetic genes encoding spider dragline silk. *Biochemistry* **34**, 10879–
529 10885 (1995).
- 530 18. Shao, Z., Vollrath, F., Sirichaisit, J. & Young, R. J. Analysis of spider silk in native and
531 supercontracted states using Raman spectroscopy. *Polymer (Guildf)*. **40**, 2493–2500
532 (1999).

533

534

Supplementary Note 1. Design of SI-Brick DNA assembly system. Our standardized SI-Brick DNA assembly system was developed based on five principle design considerations. (1) The system should allow for *in situ* iterative, back-to-back, genetic assembly of material protein repeat motifs up to the maximum genetically-permissible size. (2) The system should allow for selective swapping of the three standardized protein parts necessary for post-translational, SI-mediated ligation (i.e. RBS/Int^N, assembled material protein, and Int^C/stop codon). (3) No restriction sites within the coding sequence should introduce amino acids likely to be detrimental to SI ligation or protein material properties. (4) For maximum convenience, the platform should allow simultaneous "one-pot" assembly of all three protein parts. (5) The platform should also allow for selective swapping of the promoter, antibiotic marker, and replication origin.

We built our SI-Brick system (Supplementary Figure 1) based on existing BglBrick vectors which have been extensively used to construct multi-enzyme metabolic pathways for metabolic engineering.¹ The BglBrick vectors employ BglII and BamHI for digestion/ligation. However, the BglII and BamHI enzyme pair cannot be used to assemble material protein fragments because the resulting BglII site would introduce an arginine residue between SI and the material protein, proximal to the folded SI active site, which may negatively affect SI ligation, violating our design criterium (3). To solve this problem, we further incorporated an additional and orthogonal pair of restriction sites Nhel and Spel for iterative assembly of repetitive material protein sequences. Nhel and Spel code amino acids Alanine-Serine and Threonine-Serine, respectively, which should not affect SI ligation. During repetitive silk assembly, the scar sequence from Nhel/Spel ligation is ACTAGC, encoding a Threonine-Serine linker that is abundant in the native spidroin sequence and does not affect silk properties. Additionally, because existing BglBricks vectors already have Spel for swapping of selection markers, flanking material proteins with Nhel/Spel alone would fail to meet criterium (2). Thus, we chose to flank material protein parts with an additional pair of restriction sites (KpnI and Kpn2I), allowing the repetitive proteins to be specifically swapped by enzyme pair KpnI and Kpn2I.

To use our SI-Brick DNA assembly system, repeat material protein motifs can be iteratively assembled through back-to-back digestion/ligation using Nhel and Spel (Supplementary Figure 2). The assembled material protein sequence can then be assembled with desired SI parts, promoters, vector backbones using corresponding restriction enzymes in one step (Supplementary Figure 2e). When needed, assembled repetitive proteins can be swapped with other material proteins with KpnI/Kpn2I digestion/ligation. Cfa Int^C (including start codon and RBS) can be swapped with other Int^C or N-terminal sequences with EcoRI/KpnI digestion/ligation. Cfa Int^N can be swapped with other Int^N with or without C-terminal purification tags using Kpn2I/BamHI digestion/ligation. Promoter parts can be swapped by AatII/EcoRI digestion/ligation, antibiotic markers together with replication origin can be swapped by AatII/Xhol. In addition, when needed, other proteins (e.g. a fluorescent reporter protein) can be cloned to the same operon with, but not genetically fused to, material proteins for tracking or regulation purposes using EcoRI/BglII or BamHI/Xhol digestion/ligation.

Supplementary Table 1. Primers, UTRs, and coding sequences used in this study

Primer/ UTR/ Coding Sequence	Name	Sequence	Purpose
5'-UTR	NA	ATCAGCAGGACGCACTGACCGAATTCAAAGATTTAAGAAGGGAGATATACT	Previously optimized 5' UTR including strong RBS for high rate of translation initiation
3'-UTR	NA	GGATCCAAACTCGAGTAAGGATCTCCAGGCATCAAATAAACGAAAGGCTCAGT CGAAAGACTGGGCCTTCGTTTATCTGTTGTTGCGGTGAACGCTCTACTA GAGTCACACTGGCTCACCTCGGGTGGGCGCTTCTGCG	Previously optimized 3' UTR included two strong transcription terminators (<i>rrnB T1</i> and <i>T7Te</i>)
CDS	MaSp1 1- mer	GGTACCGCTAGCGTCGCGGTGGCTCTGGCGGTCAAGGTGCAGGTATGGCAGC AGCTGCAGCTATGGTGGCGCTGGTCAAGGGGGTATGGCGGTCTGGTAGCC AAGGCACTAGTCCGGA	Restriction site flanked 1-mer for assembly of 64-mer and 96-mer
CDS	Cfa ^N	TCCGGAGCAGAATATTGCCCTGTCTTACGACACAGAGATTGACCGTTGAATAT GGATTCCTCCATCGGTAAAGATCGTGGAGGAACGGATTGAATGCACAGTCTAT ACGGTAGATAAAAATGGTTTGTTGTTGATACACAACCTATTGCTCAGTGGCATAACC GGGGAGAACAGGAAGTTTCGAATACTGCTTAGAAGACGGTTGATTATCCGTG CAACGAAAGATCACAAATTATGACGACGGCAGGGTCAAGTTGATGGTTGCCGTAAAGGAT CC	Final optimized C-terminal SI sequence for assembly with 64-mer or 96-mer silk sequences
CDS	Cfa ^C	AGATCTTTAAGAAGGGAGATATACATATGGCTAAGACTAAAGTCAGATCATTA GTCGTAAGAGTCTGGCACTAAAACGTCAGATATTGGAGTAGAAAAAGATC ATAATTTTTGCTGAAGAATGGGCTGGTGGCCTAACTGCTTCAACGGTACCC	Final optimized N-terminal SI sequence for assembly with 64-mer or 96-mer silk sequences
Primer	GlyV-F	CGGAACGACGTCAATTTCCTGGTCACGTAAGCG	Amplification of GlyV from <i>E. coli</i> genome and cloning into pAk backbone
Primer	GlyV-R	GGCTACCTCGAGTTGGTGGTCTGTGCTTGCAAG	Amplification of GlyV from <i>E. coli</i> genome and cloning into pAk backbone

Supplementary Table 2. Plasmids used in this study

Plasmid Name	ORI	Promoter	Resistance	Gene	Plasmid Source
pB6c	pBBR1	P _{LlacO1}	Cm ^R	-	Anderson et al. 2010 ¹
p96	pBBR1	P _{LlacO1}	Cm ^R	96-mer	Present study
p64 ^N	pBBR1	pLlacO1	Cm ^R	64-mer + optimized 3' Cfa ^N	Present study
p ^C 64	pBBR1	pLlacO1	Cm ^R	64-mer + optimized 5' Cfa ^C	Present study
p96 ^N	pBBR1	pLlacO1	Cm ^R	96-mer + optimized 3' Cfa ^N	Present study
p ^C 96	pBBR1	pLlacO1	Cm ^R	96-mer + optimized 5' Cfa ^C	Present study
pA2k	p15A	P _{Tet}	Kan ^R	-	JBE BioBrick paper
pGlyV	p15A	Native glyV,X,Y promoter	Kan ^R	Native <i>E. coli</i> glyV and promoter	Present study

Supplementary Table 3. Strains used in this study

Strain Name	Genotype	Strain Source
NEB10 β	$F' proA+B+ lacIq$ $\Delta(lacZ)M15 zzf::Tn10$ $(TetR) \Delta(ara-leu) 7697$ $araD139 fhuA \Delta lacX74$ $galK16 galE15 e14-$ $\phi80dlacZ\Delta M15 recA1$ $relA1 endA1 nupG rpsL$ $(StrR) rph spoT1 \Delta(mrr-hsdRMS-mcrBC)$	NEB
s96	NEB10 β containing p96 + pGlyV	Present study
s64 ^N	NEB10 β containing p64 ^N + pGlyV	Present study
s ^C 64	NEB10 β containing p ^C 64 + pGlyV	Present study
s96 ^N	NEB10 β containing p96 ^N + pGlyV	Present study
s ^C 96	NEB10 β containing p ^C 96 + pGlyV	Present study

Supplementary Table 4. Diameter measurements and mechanical properties for 96-mer fibers

FIBER	Diam. A (μm)	Diam. B (μm)	Diam. C (μm)	Avg. Diameter (μm)	σ (MPa)	E (GPa)	ϵ (%)	U_T (MJ/m ³)
1	6.53	6.22	5.57	6.11	566.7	7.4	25.4	110.0
2	5.89	6.22	5.58	5.90	526.6	7.6	21.8	90.0
3	7.80	7.33	7.48	7.54	401.3	5.6	26.7	90.0
4	6.69	7.21	7.50	7.13	520.8	8.1	33.0	130.0
5	6.53	5.93	6.40	6.29	475.2	6.9	32.2	120.0
6	5.91	6.05	6.85	6.27	447.9	6.6	22.9	70.0
7	7.86	6.38	8.61	7.62	515.4	8.7	36.1	140.0
8	6.24	6.08	6.69	6.34	558.8	8.9	15.3	60.0
9	5.58	5.26	5.42	5.42	672.2	8.6	21.7	110.0
10	5.57	4.94	5.10	5.20	670.3	9.8	18.3	90.0
11	6.58	7.35	6.42	6.78	397.1	5.3	15.6	40.0
12	5.42	6.53	6.42	6.12	504.4	7.8	16.2	60.0
13	5.42	5.73	6.05	5.73	574.3	9.1	22.1	100.0
14	6.21	6.53	5.42	6.05	524.3	9.1	16.2	60.0

Supplementary Table 5. Diameter measurements and mechanical properties for 128-mer fibers

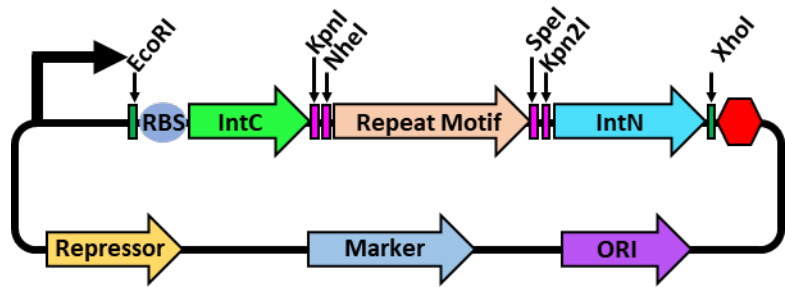
FIBER	Diam. A (μm)	Diam. B (μm)	Diam. C (μm)	Avg. Diameter (μm)	σ (MPa)	E (GPa)	ϵ (%)	U_T (MJ/m ³)
1	7.33	7.05	6.63	7.00	874.4	11.4	39.2	260.0
2	6.56	7.68	6.03	6.76	886.1	9.5	18.9	100.0
3	7.96	5.47	5.65	6.36	650.2	8.4	12.7	50.0
4	7.49	5.87	6.00	6.45	652.1	8.0	29.5	150.0
5	4.98	3.54	4.66	4.39	642.9	12.9	9.5	40.0
6	7.18	6.42	7.07	6.89	877.2	12.6	33.3	200.0
7	6.76	6.91	6.34	6.67	654.3	9.0	19.4	80.0
8	5.77	5.74	6.55	6.02	843.0	9.5	16.8	90.0
9	6.36	6.53	5.75	6.21	816.2	10.7	15.2	110.0
10	7.01	6.85	7.66	7.17	750.4	9.6	22.0	90.0
11	7.91	7.91	7.37	7.73	744.8	8.2	27.3	130.0
12	6.41	5.65	5.59	5.88	817.5	11.8	17.4	90.0
13	6.69	7.50	8.13	7.44	717.0	10.7	25.5	120.0
14	7.41	8.51	8.20	8.04	816.7	12.3	20.0	100.0

Supplementary Table 6. Diameter measurements and mechanical properties for 128-mer fibers

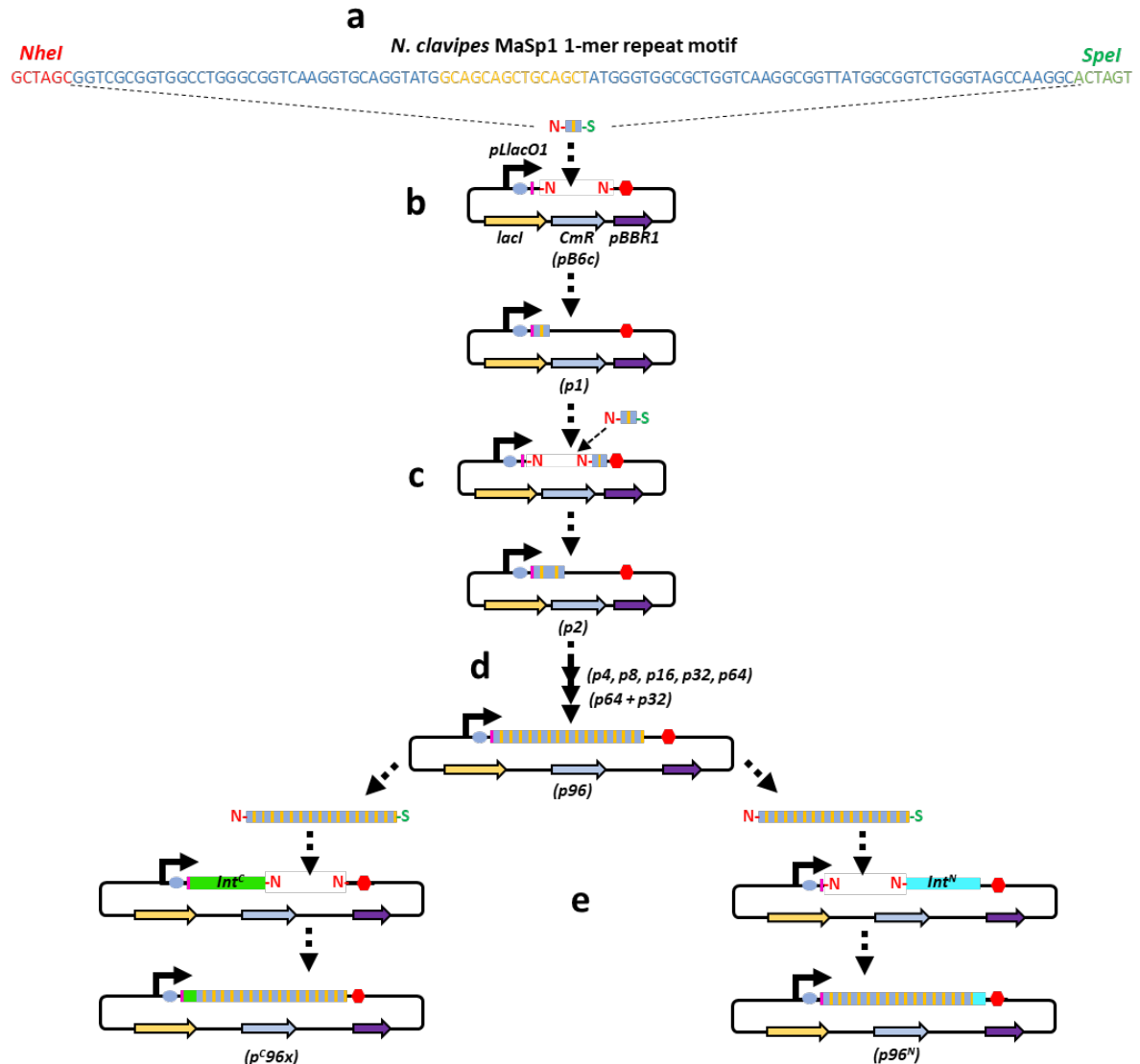
FIBER	Diam. A (μm)	Diam. B (μm)	Diam. C (μm)	Avg. Diameter (μm)	σ (MPa)	E (GPa)	ϵ (%)	U_T (MJ/m ³)
1	3.02	3.04	2.75	2.94	1078.6	14.7	11.7	70.0
2	6.56	7.68	7.34	7.19	892.9	9.0	15.3	70.0
3	4.98	7.41	7.37	6.59	1034.8	17.8	28.0	200.0
4	6.91	6.89	6.72	6.84	1135.6	11.8	17.7	110.0
5	7.32	7.33	7.64	7.43	911.5	12.2	14.0	80.0
6	6.34	5.50	6.13	5.99	1324.6	18.9	27.2	220.0
7	3.19	3.38	3.06	3.21	1130.5	17.2	15.6	100.0
8	5.25	5.89	5.10	5.41	982.8	10.5	18.4	100.0
9	4.80	5.12	5.81	5.24	987.6	10.3	24.6	140.0
10	5.73	5.73	7.01	6.16	1003.0	14.3	12.2	70.0
11	5.65	5.91	6.15	5.90	961.7	14.5	21.8	140.0
12	5.78	5.91	5.92	5.87	1016.0	11.9	12.1	70.0
13	6.53	5.89	5.57	6.00	1016.6	13.1	12.8	70.0
14	5.09	5.29	4.94	5.11	952.4	15.2	24.3	160.0

Supplementary Table 7. Quantification of morphological differences between fibers of different molecular weight.

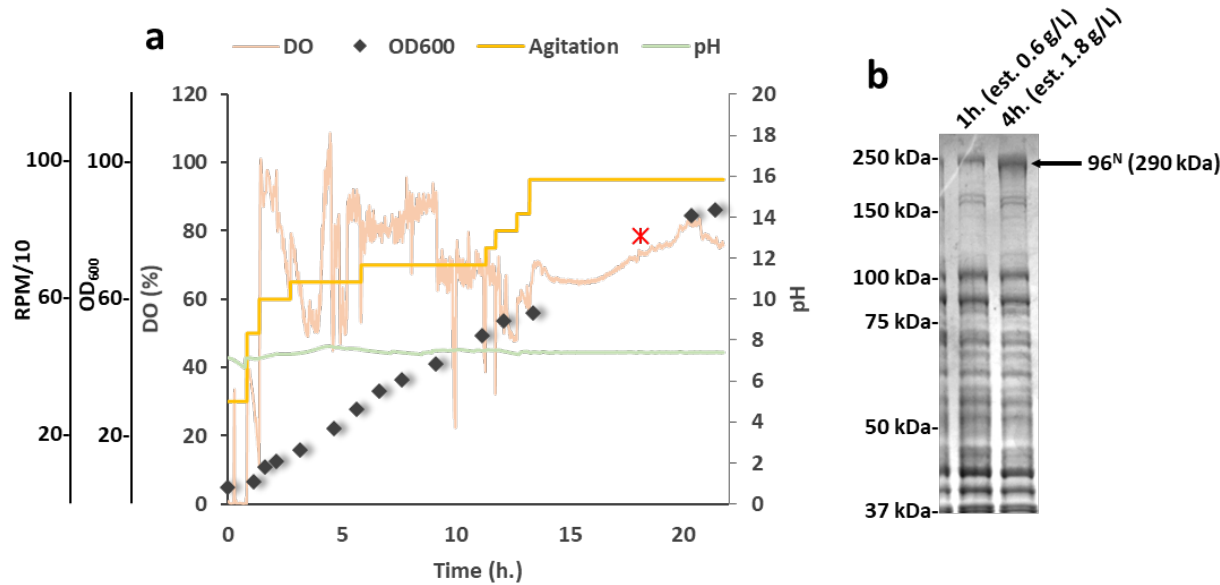
Fiber	Circularity	Surface Roughness	Interior Roughness
96-mer	0.55 ± 0.14	4.17 ± 0.68	8.17 ± 0.98
128-mer	0.82 ± 0.10	1.75 ± 0.69	7.17 ± 0.75
192-mer	0.89 ± 0.05	1.08 ± 0.58	5.08 ± 0.80



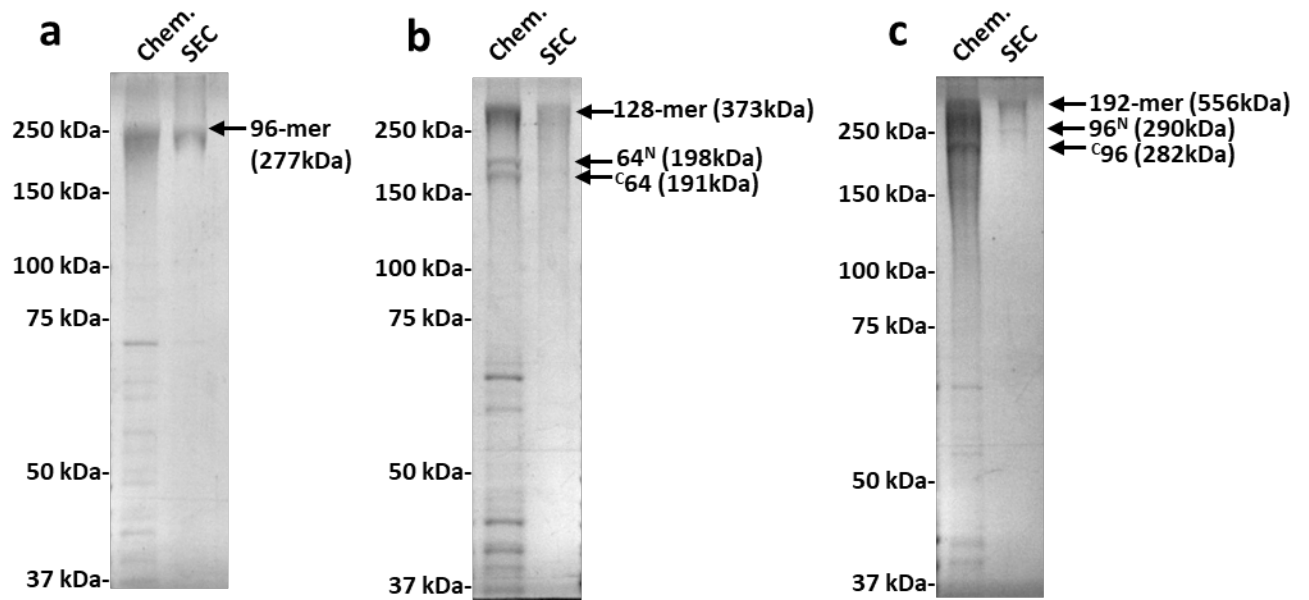
Supplementary Figure 1. SI-Bricks assembly system. The SI-Bricks assembly system allows for iterative assembly of repeat motifs through back-to-back NheI/SpeI digestion/ligation (Supplementary Figure 2). Assembled PBM parts are swapped with KpnI/Kpn2I digestion/ligation, Int^C parts (including start codon and RBS) are swapped with EcoRI/KpnI digestion/ligation, and Int^N parts are swapped with Kpn2I/XbaI digestion/ligation.



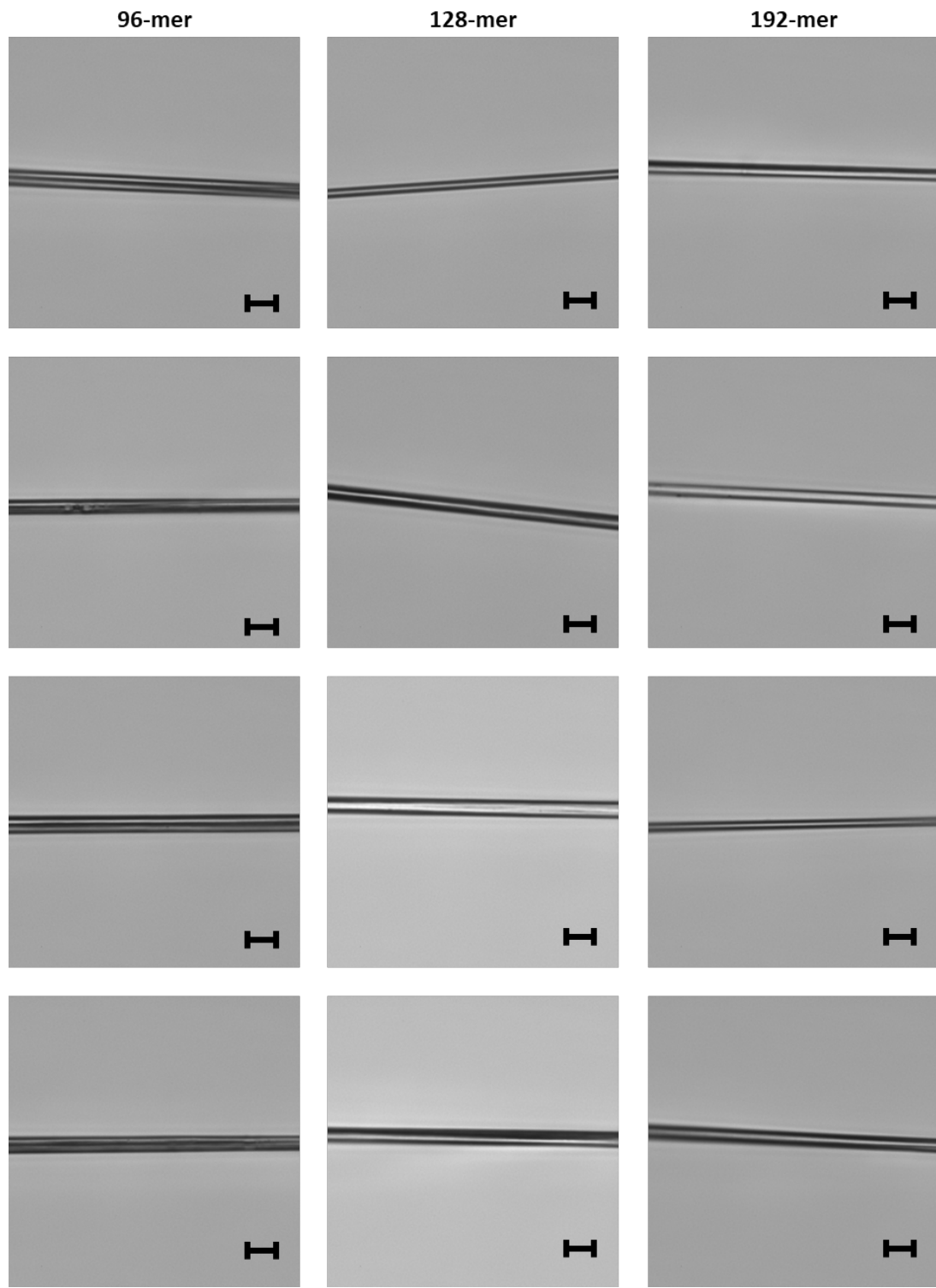
Supplementary Figure 2. Schematic of iterative assembly of plasmids. (a) The optimized coding sequence for a single representative repeat unit (1-mer) of the *N. clavipes* dragline silk MaSp1 protein is flanked by restriction sites *NheI* (N) and *SpeI* (S). (b) The sequence is ligated into the BglBricks vector pb6c with IPTG-inducible promoter *pLlacO1*, replication origin *pBBR1*, and chloramphenicol resistance *Cm^R*. (c) After selection for correct insert orientation, the resulting 1-mer plasmid (p1) is linearized by digestion with *SpeI*. The linearized vector is ligated with 1-mer insert to yield p2. (d) The process is repeated, each time with a two-fold larger insert until p64 is obtained. Plasmid p96 was obtained by inserting *NheI/SpeI* digested 32-mer into linearized p64. (e) The 96-mer is then inserted either 5' of optimized *Int^N* to yield p96^N or 3' of optimized *Int^C* to yield p^{C96x}.



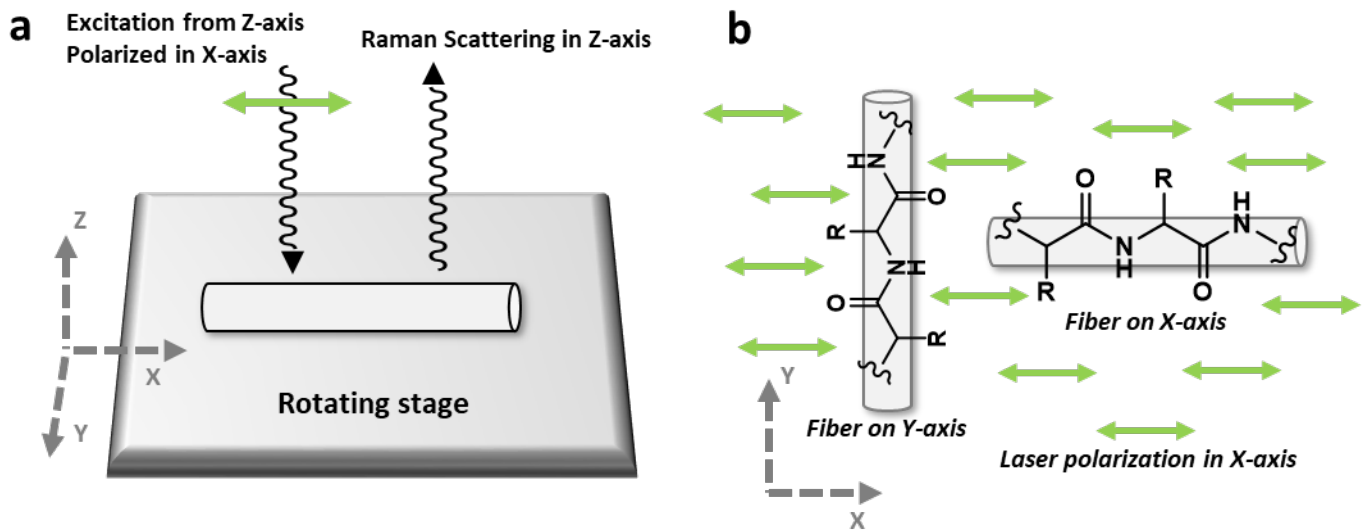
Supplementary Figure 3. Bioproduction of spidroins in fed-batch bioreactor. (a) Dissolved oxygen (DO), cell density (OD₆₀₀), bioreactor agitation rate, and pH over the course of fermentation. Time 0 represents the start of fermentation in the bioreactor. The red asterisk indicates the point of induction with 1 mM IPTG. (b) Representative SDS-PAGE of spidroin-producing cells (96^N) at 1 and 4 h post induction. Estimated titers of 96^N are indicated above each lane. Titers were estimated based on densitometric analysis of the SDS-PAGE gel as described in the methods.



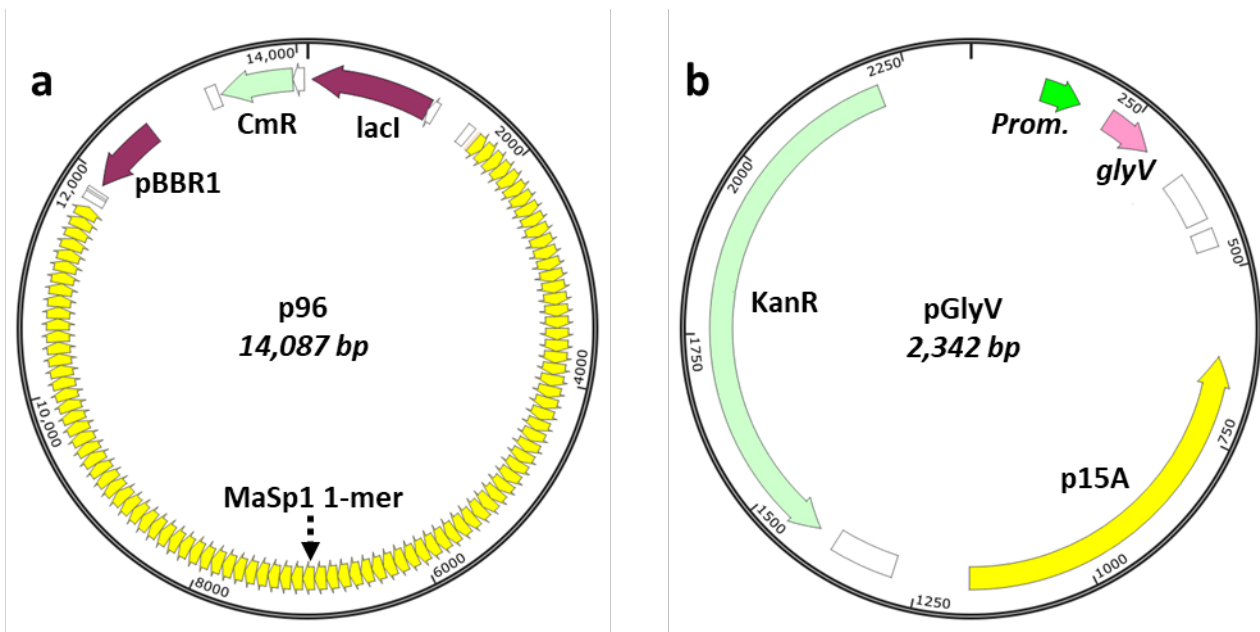
Supplementary Figure 4. Purification of 96, 128, and 192-mer spidroins. Coomassie Blue stained SDS-PAGE gels for purification of (a) 96-mer, (b) 128-mer, (c) 192-mer. Lane 1, products after selective precipitation with ammonium sulfate. Lane 2, products after SEC purification.



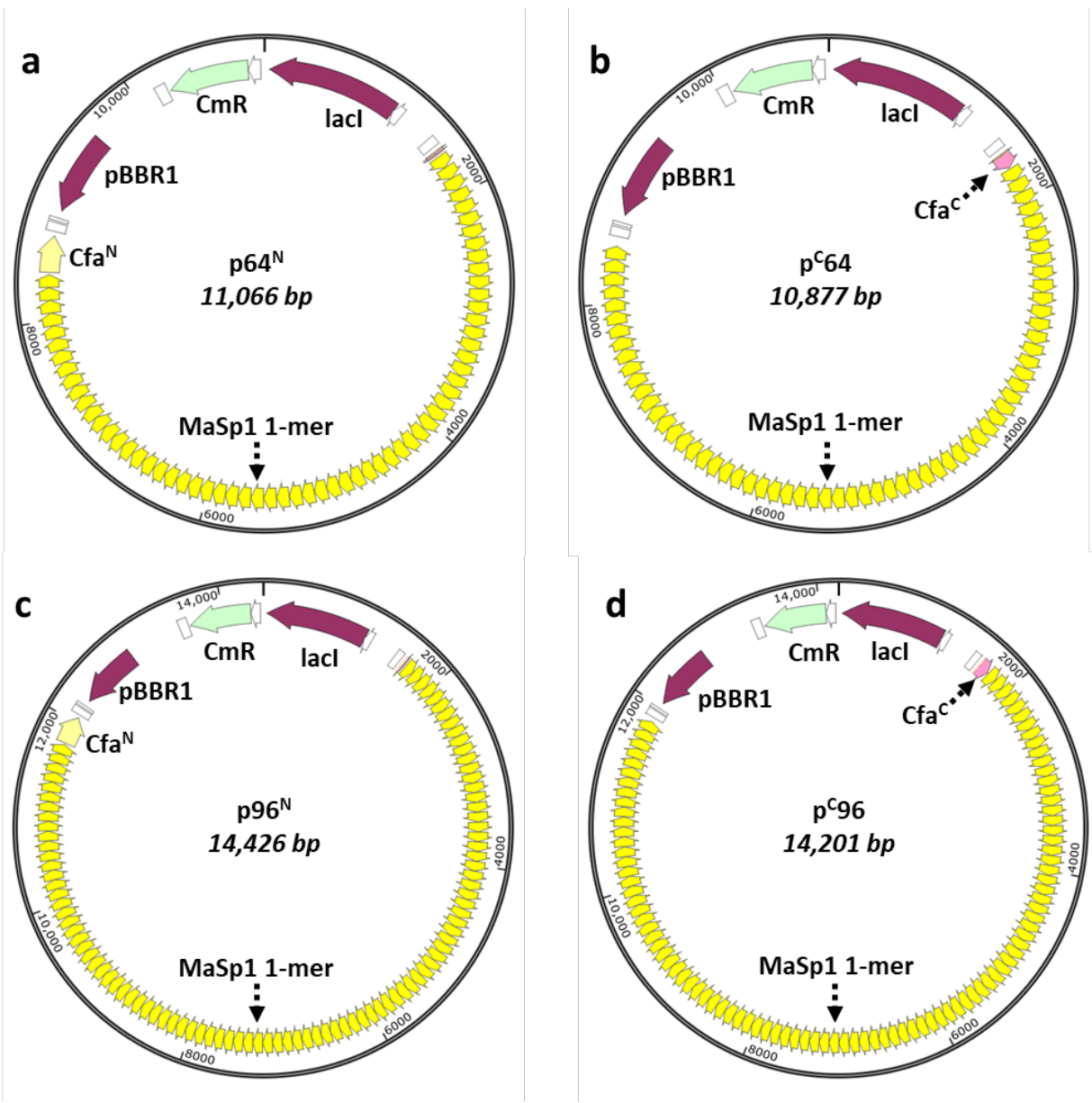
Supplementary Figure 5. Light microscopy of spun spidroin fibers. Representative images of spidroin fibers were recorded using a Nikon Eclipse TiE Inverted Microscope and a 60x objective. Scale bar is 5 μ m.



Supplementary Figure 6. Polarized Raman microspectroscopy. **(a)** Schematic representation of the apparatus from a side view. The fiber is mounted along the X-axis of a rotating stage. A laser polarized in the X-axis is directed to the fiber along the Z-axis. Raman scattering is collected along the Z-axis. **(b)** Schematic representation of polarized light interaction with fibers oriented along the Y-axis (left) or X-axis (right). If peptide chains are aligned with the fiber axis (as depicted), carbonyl bonds will be maximally aligned with laser polarization when fibers are oriented along the Y-axis and minimally aligned when fibers are oriented along the X-axis. Because absorbance in the amide I band is due primarily to carbonyl stretching, an increase in 1670 cm^{-1} peak intensity when fibers are oriented along the Y-axis is indicative of β -sheet alignment parallel to the fiber axis. Thus, the normalized peak intensity ratio ($I \frac{Y}{X}$) is indicative of the degree of orientation.



Supplementary Figure 7. p96 and pGlyV plasmid maps. "Prom." indicates native *E. coli* glyV,X,Y promoter.



Supplementary Figure 8. Plasmid maps for p64^N (a), p^c64 (b), p96^N (c), p^c96 (d).

REFERENCES:

- Anderson, J. C. et al. BglBricks: A flexible standard for biological part assembly. *J. Biol. Eng.* **4**, 1–12 (2010).